Transactions of the Indian Ceramic Society

ISSN: 0371-750X (Print) 2165-5456 (Online) Journal homepage: https://www.tandfonline.com/loi/tcer20

Synthesis, Impedance and Dielectric Studies of Double Doped Strontium Bismuth Niobate Ferroelectric Ceramics

Bacchupalli Ravi Kumar, Nandiraju Venkata Prasad, Guduru Prasad & Gobburu Subramanyam Kumar

To cite this article: Bacchupalli Ravi Kumar, Nandiraju Venkata Prasad, Guduru Prasad & Gobburu Subramanyam Kumar (2019) Synthesis, Impedance and Dielectric Studies of Double Doped Strontium Bismuth Niobate Ferroelectric Ceramics, Transactions of the Indian Ceramic Society, 78:2, 89-93, DOI: 10.1080/0371750X.2019.1610068

To link to this article: https://doi.org/10.1080/0371750X.2019.1610068

Trans. Ind. Ceram. Soc., vol. 78, no. 2, pp. 89-93 (2019).

ISSN 0371-750X (Print), ISSN 2165-5456 (Online)
http://dx.doi.org/10.1080/0371750X.2019.1610068

Synthesis, Impedance and Dielectric Studies of Double Doped Strontium Bismuth Niobate Ferroelectric Ceramics

Bacchupalli Ravi Kumar, Nandiraju Venkata Prasad, Guduru Prasad and Gobburu Subramanyam Kumar*

Department of Physics, Osmania University, Hyderabad – 500 007, India

[MS received November 17, 2017; Revised copy received March 17, 2019; Accepted April 16, 2019]

ABSTRACT

Strontium bismuth niobate ($SrBi_2Nb_2O_9$ (SBN), $K_{0.025}Sr_{0.95}Gd_{0.025}Bi_2Nb_2O_9$ (KSGBN1), $K_{0.05}Sr_{0.9}Gd_{0.05}Bi_2Nb_2O_9$ (KSGBN2) and $K_{0.1}Sr_{0.8}Gd_{0.1}Bi_2Nb_2O_9$ (KSGBN3)) ceramics were prepared by two stage solid state reaction method. Calcination was done at 850°C for 4 h. Structural property of calcined samples was studied by powder X-ray diffraction (XRD) technique at room temperature. XRD patterns of the samples so obtained matched well with the reported data (ICSD #82280). Lattice parameters of the samples were calculated using POWD software. Pellets of 10 mm diameter and ~1 mm thickness were prepared using uniaxial hydraulic press at 10 MPa pressure. These pellets were finally sintered at 950°C for 4 h. The surface morphology of the samples was studied with scanning electron microscope (SEM). The density of the sintered ceramics was measured by Archimedes principle. Impedance variation with temperature was studied for SBN, KSGBN1, KSGBN2 and KSGBN3 in the frequency range of 100 Hz to 1 MHz. The temperature dependence of dielectric properties of SBN, KSGBN1, KSGBN2 and KSGBN3 were obtained at some set frequencies in the range of 100 Hz to 2 MHz using HP 4192A impedance analyzer. The data obtained was analyzed based on change in tolerance factor, anisotropy and strain due to the presence of doped impurities. Interesting conclusions arrived at have been presented.

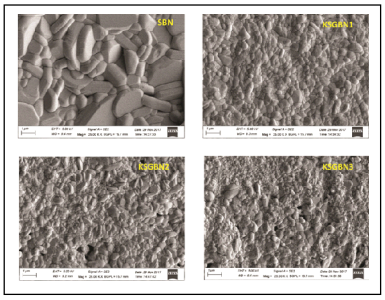

[Keywords: Ferroelectrics, XRD, SEM, Density, Impedance and Dielectric]

Introduction

In the manufacturing and usage of electronic devices, such as nonvolatile ferroelectric random access memories (NVFeRAM), capacitors, piezoelectric sensors, resonators, pyroelectric infrared detectors and optical switches,[1–3] there has been a lot of demand for ferroelectric materials due to their electrical, mechanical and optical characteristics. On account of their read-write speed, non-volatility, low operating power and radiation hardness, NVFeRAMs are promising candidates for replacing silicon based semiconductor memories due to large remnant polarization (P_r), low coercive field (E_c) and long fatigue endurance against repeated polarization switching, etc.[4] Though, lead zirconate titanate (PZT) has been investigated extensively and found to be a suitable material for NVFeRAM applications, it suffers from the toxic nature of lead (Pb), fatigue, ageing and leakage current.[5, 6]

Bismuth oxide layered structures (BLSFs) are alternate ferroelectric materials for NVFeRAM applications. These materials are suitable candidates due to their relatively high Curie temperature (*Tc*), low dielectric dissipation and high anisotropy in the layered structure.[7] Aurivillius compounds are described by the general formula $Bi_2A_{m-1}B_mO_{3m+3}$ (m = 1, 2, 3, 4), where A is a combination of ions suitable for dodecahedral coordination and B is a combination of ions suitable for octahedral coordination.[8–10] These compounds are formed by mixture of two structural elements, viz. $[Bi_2O_2]^{2+}$ layers and perovskite-type layers having the composition $(A_{m-1}B_mO_{3m+1})^{2-}$. The advantage of BLSFs over other ferroelectric materials is that they have intermediate bismuth oxide ($(Bi_2O_2)^{2+}$) layers between the ferroelectric units $(A_{m-1}B_mO_{3m+1})^{2-}$. Extensive research works[8–10] on $SrBi_2Ta_2O_9$ (SBT), and $SrBi_2Nb_2O_9$ (SBN) of the family of these layered compounds with m = 2, proved them to be versatile materials for NVFeRAM applications. The fatigue-free behavior of SBT, reported by Araujo *et al.*,[7] has gained importance among lead-free ferroelectric materials for electronic memory applications.

Many people have attempted to enhance the properties of SBN by partially substituting A and B sites with elements like barium, lanthanum, yttrium, etc.[11–17] In the present work an attempt has been made to further enhance the applicability of SBN as NVFeRAM material by partially substituting the A site (strontium) with monovalent potassium and trivalent gadolinium. While choosing these elements for doping, their ionic radii and electronegativity values have been taken into account. The ionic radii[18] of K, Sr and Gd are 1.64, 1.18 and 1.11 Å and electronegativity

*Corresponding author; email: gobburusk@gmail.com

values are 0.8, 1.0 and 1.2 eV, respectively. So, ionic radius of K is larger than those of Sr and Gd, and electronegativity of K is less than those of Sr and Gd.

Experimental

Strontium bismuth niobate (SBN, KSGBN1, KSGBN2 and KSGBN3, i.e. $SrBi_2Nb_2O_9$, $K_{0.025}Sr_{0.95}Gd_{0.025}Bi_2Nb_2O_9$, $K_{0.05}Sr_{0.9}Gd_{0.05}Bi_2Nb_2O_9$ and $K_{0.1}Sr_{0.8}Gd_{0.1}Bi_2Nb_2O_9$, respectively) ceramics were prepared by two stage solid state reaction method. Mixtures of $SrCO_3$, Bi_2O_3, Nb_2O_5, K_2CO_3 and Gd_2O_3 of purity about 99.9%, supplied by Sigma-Aldrich were used as the starting materials. These chemicals were weighed in stoichiometric proportion and thoroughly ground in agate mortar for 6 h (with excess 3% of Bi_2O_3 taken for compensating evaporation loss). The powder was then calcined at 850°C for 4 h. Calcined powder was sieved in a test sieve of BSS 400 grade for uniformity in grain size. The powder was admixed with poly vinyl alcohol (PVA) binder and pressed into pellets of 10 mm diameter and 1 to 2 mm thickness by uniaxial pressing in hydraulic jack, at an applied pressure of ~10 MPa and at room temperature (RT). These pellets were then sintered for 4 h at 950°C. Phase formation of the samples was verified by X-ray powder diffraction (XRD) analysis (using PANalytical X'pert difractometer, model no. PW 3040/60). Lattice parameters and Miller indices of the formed crystals were obtained using POWD software. Theoretical densities of the samples were estimated using the volume obtained from POWD software. Experimental density of the sintered pellets was measured by Archimedes method in liquid xylene medium. Grain structure was studied from scanning electron microscopic (SEM) (Carl ZEISS EVO 18 SEM) images of the gold coated pellet surfaces. The pellets were polished and silver paste was applied on both sides as electrodes for electrical characterization. Temperature dependence of the dielectric constant (ε) was measured at different frequencies ranging from 1 kHz to 2 MHz using HP 4192A impedance analyzer in the temperature range from RT to 480°C. Complex AC conductivity behavior was measured using AUTOLAB (PGSTAT 30) and NOVA software of version 1.11 in the temperature range of 100° to 525°C in steps of 25°C and frequency range of 100 Hz to 1 MHz in 50 steps.

Results and Discussion

Structural Properties

XRD patterns of the samples (standard SBN (ICSD # 82280), SBN, KSGBN1, KSGBN2 and KSGBN3) are shown in Fig. 1a. XRD peaks of all these samples matched with the peaks of standard SBN with orthorhombic structure and no additional noticeable peak was observed except three peaks of Bi_2O_3 corresponding to (012), (041) and (241) due to 3% excess Bi_2O_3 left unreacted after calcination. It indicates that the elements potassium (K) and gadolinium (Gd) were well diffused into SBN lattice and a new single phase solid solution was formed which belongs to Aurivillius family of ceramics with m = 2. Magnified view of the XRD pattern in the proximity of highest intensity peaks is shown in Fig. 1b. The 2θ value of the intense peak (h k l : 1 1 5) slightly decreased as the percentage of doping increased. This indicates increasing inter-planar spacing for (1 1 5) plane.[19] This may be attributed to relatively larger ionic radius of doped element K than the space available to *A* (Sr) site. Peak broadening is also observed, indicating the presence of strain in the lattice. The ionic radius of dopant K is larger and that of Gd is smaller than the original ion Sr. Smaller doping concentration produced some strain in the crystal structure. On increasing the doping concentration the effect of strain in the structure got decreased. The decrease in strain on increasing the doping level may be due to mutual compensation by the dopants. Figure 2 shows the variation of 2θ of intense peak in XRD patterns of SBN, KSGBN1, KSGBN2 and KSGBN3 with varying doping concentration. It reveals that smaller concentration of doping (0.025) produced a noticeable shift in 2θ of the intense peak (decreased from 29.03° to 28.71°) and an increase in concentration from 0.025 to 0.05 did not affect much to the 2θ (Fig. 2). Moreover, when the concentration was increased from 0.05 to 0.1 the 2θ increased slightly from 28.68° to 28.73° indicating turnaround in the structural distortion. The *b/a* ratios of lattice parameters given in Table I also indicate the same.

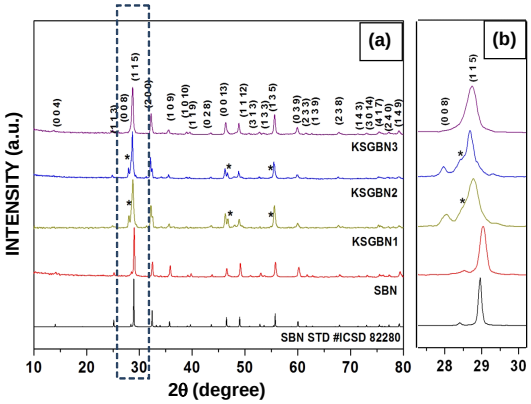

Fig. 1 – (a) XRD patterns of standard SBN (ICSD #82280), SBN, KSGBN1, KSGBN2 and KSGBN3, (b) magnified portions of the intense peaks (*: peaks of Bi_2O_3)

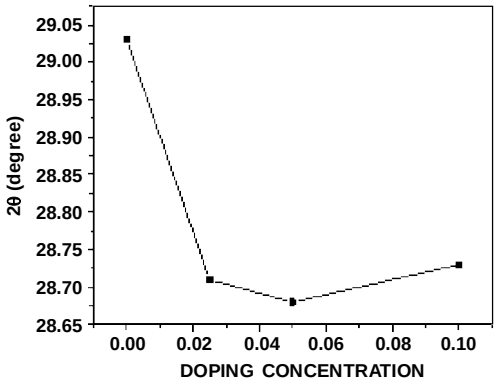

Fig. 2 – Variation of 2θ of intense peak in XRD patterns of SBN, KSGBN1, KSGBN2 and KSGBN3 with the variation in doping concentration

Table I : Comparison of lattice parameters, theoretical and experimental densities of the prepared samples of SBN, KSGBN1, KSGBN2 and KSGBN3

Sample name	Lattice parameters			*b/a*	Unit cell volume ($Å^3$)	Theoretical density ($g.cm^{-3}$)	Experimental density ($g.cm^{-3}$)	Density (%)	γ of modified Curie-Weiss law at 100 kHz
	a (Å)	*b* (Å)	*c* (Å)						
SBN from ICSD	5.518	5.515	25.112	0.999	764.39	7.26	–	–	–
SBN (doping 0.0)	5.523	5.508	25.032	0.997	761.64	7.29	6.99	95.93	1.06
KSGBN1 (doping 0.025)	5.546	5.513	25.139	0.994	768.85	7.21	6.23	86.36	1.12
KSGBN2 (doping 0.050)	5.549	5.507	25.019	0.992	764.63	7.26	6.50	89.49	1.74
KSGBN3 (doping 0.10)	5.541	5.513	25.439	0.995	777.22	7.15	6.86	95.99	1.72

Lattice parameters *a*, *b*, *c* and unit cell volume *V* of the samples obtained from POWD software are shown in Table I. Theoretical density of the samples was calculated and compared with the values obtained from Archimedes principle. Porosity decreased with increasing doping concentration. Average size of crystallites (*B*) of the prepared samples are calculated using Scherrer's formula:[20] $B(2\theta) = k\lambda/L\cos\theta$, where *k* is a constant, λ is the X-ray wavelength, θ is Bragg's angle and *L* is full width at half maximum, calculated assuming Gaussian nature of the XRD peak. The crystallite size values thus obtained were 92.683, 54.162, 22.082, 34.290 and 28.886 nm for standard SBN (from ICSD), SBN, KSGBN1, KSGBN2 and KSGBN3, respectively. SEM pictures shown in Fig. 3 confirm the existence of porosity in the samples and decrease in grain size. Randomly oriented disc like grains are observed in the SBN samples. The grain size decreased as the doping concentration increased for the same sintering temperature and time. This indicates that grain growth is hindered by doping. This may be due to relatively smaller impurity ions (Gd) inducing more buckling in the bond angle and smaller tolerance factor[21] restricting the diffusion of parent ions resulting in smaller grains.

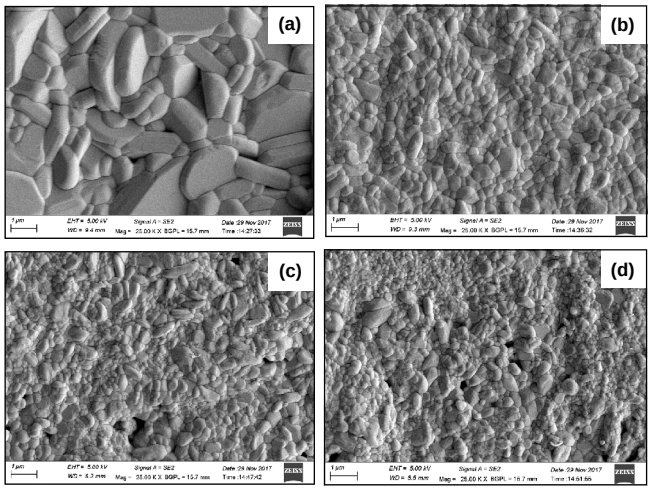

Fig. 3 – SEM images of (a) SBN, (b) KSGBN1, (c) KSGBN2 and (d) KSGBN3

Electrical Properties

Dielectric Properties

Temperature dependence of dielectric constant, ε, measured at 10, 100 and 1000 kHz frequencies from RT to 480°C temperature is shown in Fig. 4. For all the samples the ε value is ~100 at RT. Ferroelectric materials are characterized by a transition temperature called Curie temperature (T_C) at which the ε is maximum. T_C value decreased from 450°C (for KSGBN1) to 441°C (for KSGBN3) on increasing the doping concentration from 0.025 to 0.10. Relaxer nature of the prepared samples can be analyzed from modified Curie-Weiss relation shown in Eqn (1):[22]

$$\frac{1}{\varepsilon} - \frac{1}{\varepsilon'} = \frac{(T - T_{max})^{\gamma}}{C'} \qquad ..(1)$$

Figure 5 shows $\ln\left(\frac{1}{\varepsilon} - \frac{1}{\varepsilon_{max}}\right)$ versus $\ln(T - T_C)$ graphs of SBN, KSGBN1, KSGBN2 and KSGBN3 samples at 100 kHz frequency. The γ values of modified Curie-Weiss law obtained from these graphs are given in Table I. Gradual increase in the γ value on increasing the doping concentration indicates an increase in the diffused nature in the transition from ferroelectric to paraelectric nature.

Impedance Properties

Cole-Cole plots give an insight into various relaxation mechanisms in dielectric materials arising due to various microstructural features.[23, 24] Figure 6 shows Cole-Cole plots of the prepared samples at 525°C temperature fitted with electromechanical modelling using "Z-View" software. In the standard sample SBN only two semicircles are formed, whereas for the samples KSGBN1, KSGBN2 and KSGBN3 third semicircle of very small magnitude is formed. In all the fitted curves the first semicircle is the largest; the second one is relatively smaller than the first one. Graphs in Fig. 6 indicating the impedance are mainly due to the bulk property of the crystal grains. The contribution of grain boundaries to the impedance of the material is relatively less and electrode-ceramic interface is feeble.

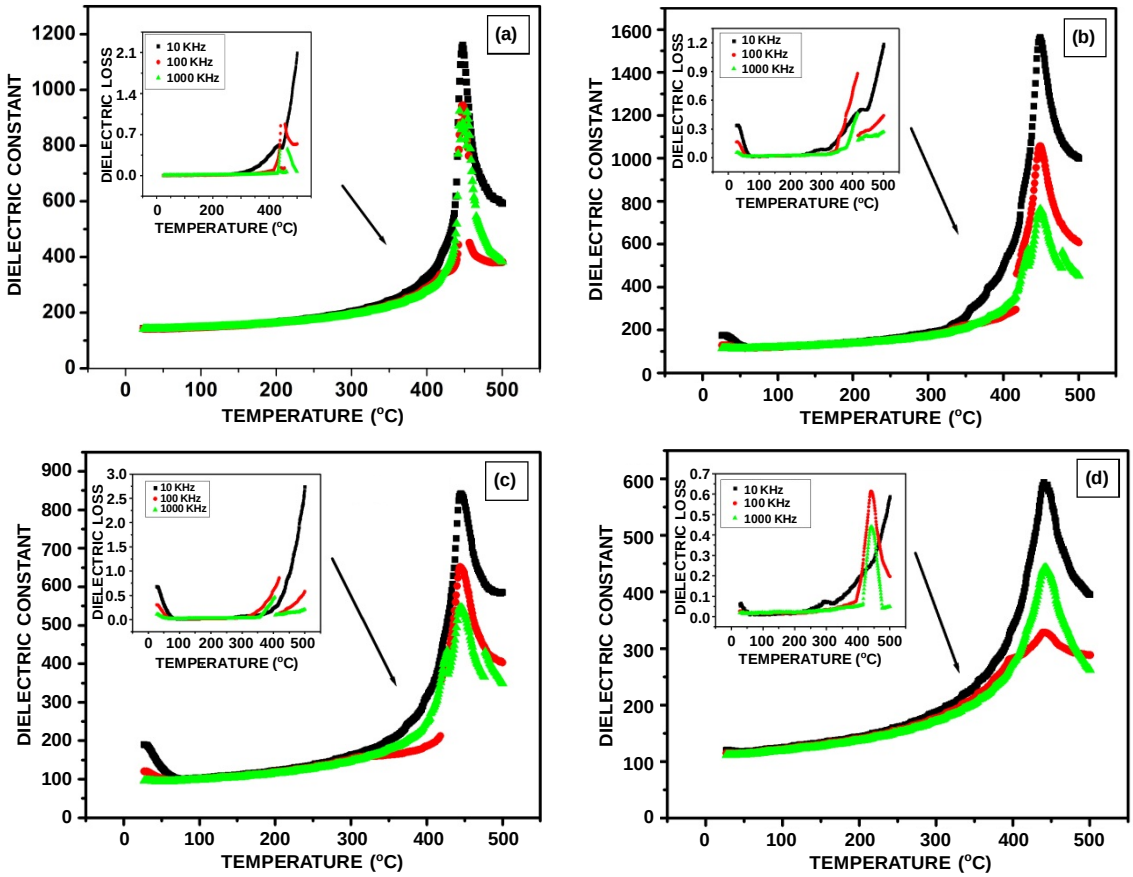

Fig. 4 – Variation of dielectric constant with temperature of (a) SBN, (b) KSGBN1, (c) KSGBN2 and (d) KSGBN3

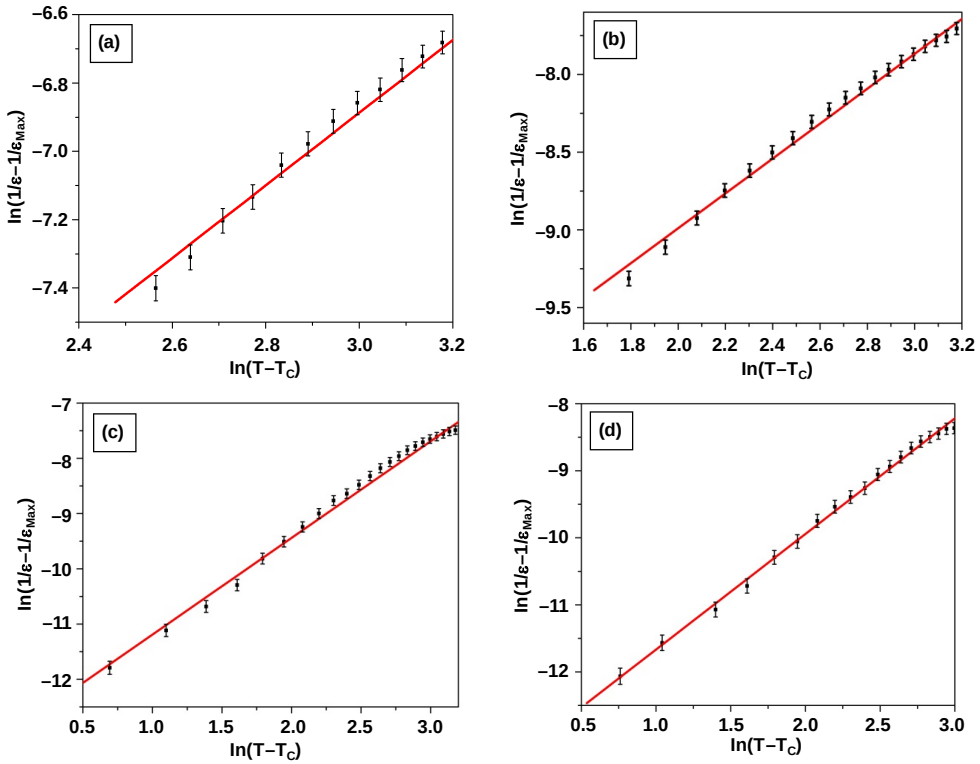

Fig. 5 – $\ln\left(\frac{1}{\varepsilon}-\frac{1}{\varepsilon_{max}}\right)$ versus $\ln(T-T_C)$ graphs of (a) SBN, (b) KSGBN1, (c) KSGBN2 and (d) KSGBN3 samples at 100 kHz frequency

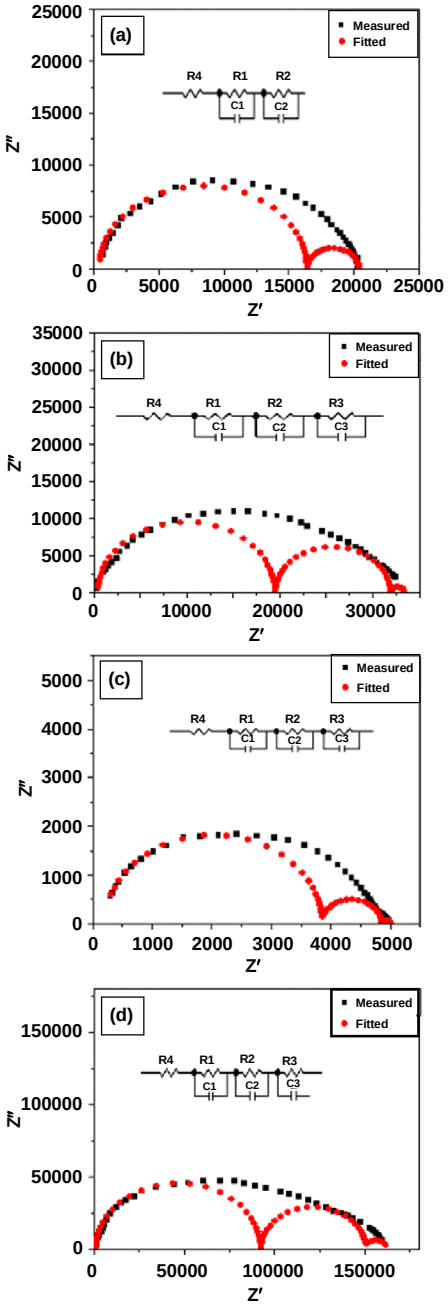

Fig. 6 – Cole-Cole plots of (a) SBN, (b) KSGBN1, (c) KSGBN2 and KSGBN3 at 525°C temperature fitted with electromechanical modelling and equivalent circuit

Conclusions

A new set of BLSF-O_9 compounds have been formed with double doping at *A* site of SBN. No extra phase was traceable and obtained the XRD confirmed pattern the presence of orthorhombic structure similar to the parent compound. SEM images showed cube like well-formed uniform grains. With increasing doping concentration, microstructure improved in forming well-defined grains. XRD showed a small shift in 2θ values, indicating the occurrence of some lattice distortion. Smaller doping concentration produced some strain in the crystal structure but on increasing the doping concentration the effect of distortion in the structure decreased. Due to lattice distortion, T_C value of the newly formed compounds decreased from 450° to 441°C for the change in doping concentration from 0.025 to 0.10. Impedance studies also showed and confirmed well-formed dense samples with 90% of theoretical density (except one compound). Complex impedance graph confirmed that the impedance of the material was mainly due to the bulk property of the material, contribution of grain boundary was smaller and the electrode interface effect was negligible. Further studies are required to completely understand their ferroelectric nature and true application suitability.

References

1. J. F. Scott and C. A. P. de Araujo, *Science*, **246**, 1400-1405 (1989).
2. J. J. Lee, C. L. Thio and S. B. Desu, *J. Appl. Phys.*, **78**, 5073-5078 (1995).
3. G. H. Haertling, *J. Vac. Sci. Tech.*, **9**, 414-420 (1990).
4. A. Kitamura, Y. Noguchi and M. Miyayama, *Mater. Lett.*, **58**, 1815-1818 (2004).
5. J. F. Chang and S. B. Desu, *J. Mater. Res.*, **9**, 955-969 (1994).
6. P. C. Joshi and S. B. Krupanidhi, *J. Appl. Phys.*, **72**, 5827-5833 (1992).
7. C. A. P. de Araujo, J. D. Cuchiaro, L. D. Macmillan, M. C. Scott and J. F. Scott, *Nature (London)*, **374**, 627-629 (1995).
8. B. Aurivillius, *Ark. Kemi*, **1**, 463-480 (1949).
9. E. C. Subba Rao, *J. Phys. Chem. Solids*, **23**, 665-676 (1951).
10. T. Kikuchi, A. Watanabe and K. Uchida, *Mater. Res. Bull.*, **12**, 299-304 (1977).
11. A. R. James, S. Balaji and S. B. Krupanidhi, *Mater. Sci. Eng.*, **B64**, 149-156 (1999).
12. T. Mihara, H. Yoshimori, H. Watanabe and C. A. P. de Araujo, *J. Appl. Phys.*, **34**, 5233-5239 (1995).
13. M. P. Dasaria, K. S. Rao, P. M. Krishna and G. G. Krishna, *Acta Phys. Pol. A*, **119**, 387-394 (2011).
14. V. Shrivastavaa, A. K. Jha and R. G. Mendiratta, *Phys. B*, **371**, 337-342 (2006).
15. Sugandha and A. K. Jha, *Ferroelectrics*, **447**, 136-142 (2013).
16. Z. Yao, R. Chu, Z. Xu, J. Hao, D. Wei and G. Li, *J. Mater. Sci.: Mater. Electron.*, **26**, 8740-8746 (2015).
17. J. D. S. Guerra, I. C. Reis, A. C. Silva, E. B. Araujo, R. Guo and A. S. Bhalla, *Integr. Ferroelectr.*, **166**, 150-157 (2015).
18. R. D. Shannon, *Acta Cryst.*, **A32**, 751-767 (1976).
19. S. N. Padmavathi, C. Sameera Devi, M. Vithal, G. Prasad and G. S. Kumar, *Ferroelectrics*, **445**, 121-135 (2013).
20. J. I. Langford and A. J. C. Wilson, *J. Appl. Cryst.*, **11**, 102-113 (1978).
21. C. H. Yang, D. Kan, I. Takeuchi, V. Nagarajan and J. Seidal, *Phys. Chem. Chem. Phys.*, **14**, 15953-15962 (2012).
22. K. Uchino and S. Nomura, *Ferroelectrics*, **44**, 55-61 (1982).
23. A. D. Brailsford and D. K. Hohnke, *Solid State Ionics*, **11**, 133-142 (1983).
24. C. Sameera Devi, M. B. Suresh, G. S. Kumar and G. Prasad, *Trans. Indian Ceram. Soc.*, **77**, 30-36 (2018).